Optimization of detection efficiency in silicon photomultipliers via topological photonic crystals*

GUO Chaoqian[1], ZHANG Guoqing[1,3,5], ZHANG Haotong[1], WU Yun[2], WANG Jun[1,3], YANG Yanfei[1,3,5], LIU Lu[1,4,5], LIU Lina[4], LI Lianbi1,3,5, HAN Xiaoxiang[1,3,5], LI Zebin[1,3,5], HAN Chao[1,3,5]

1.School of Science, Xi'an Polytechnic University, Xi'an 710048, China

2.Beijing Institute of Control Engineering, Beijing 100190, China

3.School of Science, Xi'an University of Technology, Xi'an 710048, China

4.Key Laboratory of Nuclear Protection Textile Equipment Technology, Xi'an 710048, China

5.Shaanxi Provincial Engineering Research Center for Radiation Flexible Protection Technology, Xi'an 710048, China

Abstract

Silicon photomultipliers (SiPMs) have been widely used in the field of weak light detection. However, SiPMs utilizing small-sized Geiger-mode avalanche photodiode (G-APD) cells face the limitations due to a restricted effective geometric fill sactor (GFF), which leads to relatively low photon detection efficiency (PDE), and additionally, constrained by the intrinsic properties of silicon materials, their PDE in the near-infrared band is also relatively insufficient. To address the above issues, this work proposes a regional optical field modulation approach based on topological photonic crystals (TPCs), aiming to improve the PDE of SiPMs without modifying their internal structure. Through COMSOL electromagnetic wave frequency-domain simulation, the multi-band synergistic mechanism of dead-zone topological edge state guidance, photosensitive region slow-light effect, and Bragg

---

* The paper is an English translated version of the original Chinese paper published in Acta Physica Sinica. Please cite the paper as: **GUO Chaoqian, ZHANG Guoqing, ZHANG Haotong, WU Yun, WANG Jun, YANG Yanfei, LIU Lu, LIU Lina, LI Lianbi, HAN Xiaoxiang, LI Zebin, HAN Chao, Optimization of detection efficiency in silicon photomultipliers via topological photonic crystals.** *Acta Phys. Sin.*, 2025, 74(22): 220702. DOI: 10.7498/aps.74.20250892

scattering is revealed. In the 460–700 nm band, the honeycomb lattice in the dead zone induces topological edge states via Floquet periodic analysis, while the periodic dielectric distribution of the lattice excites Bragg scattering to reduce photon reflection loss at the metal surface and precisely couples photons to the photosensitive region, leading to an increase in effective GFF from 46.4% to 63.1% at 621 nm. In the 700–1100 nm band, in addition to reducing reflection loss via Bragg scattering, the designed periodic silicon pillar structure can effectively extend the transverse propagation path of photons through the slow-light effect, thereby increasing the coupling probability with the photosensitive region, resulting in a significant increase in absorption efficiency from 41.19% to 55.94% at 900 nm. Simulation results show that this design scheme increases the average PDE of SiPMs by 50% in the 460–1100 nm band (with a peak value of 81%) and can be implemented via mainstream etching processes (electron beam lithography + reactive ion etching). Compared with traditional microlens and plasmonic structures, TPCs exhibit significant advantages in broad-spectrum response and process simplification. This work provides a new topological photonics approach for photon recycling and PDE enhancement of SiPMs.

Keywords: silicon photomultiplier, photon detection efficiency, topological photonic crystal, slow-light effect

PACS： 78.47.dc, 78.47.D–, 42.70.Qs, 42.70.Gi

doi: 10.7498/aps.74.20250892

cstr: 32037.14.aps.74.20250892

1. Introduction

Silicon photomultiplier (silicon photo multiplier, SiPM) has been widely used in the fields of high energy physics detection, nuclear medicine imaging and laser radar due to its single photon resolution and high stability at room temperature[1–3]. As the core performance index, photon detection efficiency (PDE) directly affects the signal-to-noise ratio and imaging dynamic range of the system. PDE is determined by geometric fill factor (GFF), internal quantum efficiency (IQE) and Geiger trigger efficiency (GE). GFF is limited by the dead region between adjacent Geiger-mode avalanche photodiode (G-APD) units in Geiger mode (the typical metal spacing is 2-7 μm, resulting in a dead region ratio of 20% -60% mode avalanche photodiode[4,5]), while IQE is limited by the band gap (1. 12 eV) of silicon material, which leads to low photon absorption efficiency in the near-infrared band (>1100 nm) due to the sharp decline of absorption coefficient, thus restricting the broad-spectrum detection ability of SiPM[6].

In order to improve PDE, academia and industry have proposed a variety of solutions from the dimensions of device structure optimization and working condition regulation. Haefeli et al.[7] achieved a 24% PDE improvement by redirecting incident photons from the dead zone to the active area through a checkerboard microlens layout (covering 50% of the pixels), but the sub-micron alignment accuracy requirement significantly increased the manufacturing complexity; Álvarez-Garrote et al.[8] use wavelength conversion layers, such as TPB coatings, to convert 128 nm VUV light to 425 nm visible light, maintaining more than 15% PDE at low temperatures. However, low temperature conditions not only suppress the dark count rate (DCR), but also enhance the avalanche trigger probability through carrier mobility enhancement; Villa and other[9] increase the GFF to 73.7% by optimizing the arrangement of micro-units, and achieve a peak PDE of 25.6% in the near ultraviolet band, but the dense arrangement may cause the risk of optical crosstalk; The ultra-small SiPM array developed by Yue et al.[10] has achieved high photon detection efficiency (25.4%) at the microscale through geometry optimization (41% fill factor) and material process innovation (epitaxial volume quenching technology), but the manufacturing process is complex and accompanied by yield risk.

Although the above methods improve the PDE performance of SiPM in different dimensions, they generally have some problems, such as poor process compatibility (for example, the alignment error tolerance of microlens is $< \pm 0.5$ μm), high cost (for example, low temperature packaging), and limited optical response range (for instance, the plasmonic structure only covers 50 nm band). In order to solve the above problems, a sub-regional optical field control scheme based on topological photonic crystal (TPC) is proposed in this paper: a honeycomb lattice (lattice constant 300 nm) is constructed in the dead zone, and the topological edge state is induced by Floquet periodicity analysis to realize the directional transmission of anti-scattering photons, while the periodic dielectric distribution of the honeycomb lattice excites the Bragg resonance[11], which effectively reduces the reflection loss of the metal surface and improves the photon recovery efficiency in the dead zone. A periodic silicon pillar structure (diameter $2R/3, R = a_0/2.9$) is designed in the photosensitive region to excite the slow light effect[12] and extend the transverse optical path, while Bragg scattering reduces the reflection loss, combined with the wavelength-dependent absorption coefficient of silicon material ($\alpha(\lambda)$), which can further enhance its absorption efficiency. The scheme is based on the preparation process of epitaxial layer with high resistivity on low resistivity substrate, and realizes the reconstruction of photon path with wide spectrum of 460 — 1100 nm by constructing TPC on the surface, which significantly improves the PDE of SiPM. This technology breaks through the band and process limitations of traditional microlens (400 — 900 nm) and plasmonic structure (430 — 480 nm), and can provide a new topological photonics path for highly sensitive detection of silicon-based solid-state detectors.

2. Basic principle

Based on the lattice deformation-induced **artificial time-reversal symmetry** and band inversion theory proposed in the literature [13] (without the need for Chern number calculations), this paper introduces the region-specific design of topological photonic crystals into the performance optimization of SiPM devices, taking into account the structural characteristics of SiPMs. Wu and Hu [13] systematically elucidated the regulatory mechanism of topological edge states in symmetric honeycomb photonic crystals through theoretical modeling and experimental validation. However, their study did not address the application of photon recycling in SiPM devices or the improvement of PDE.

Fig. 1(a) shows the schematic diagram of the three-dimensional structure of the SiPM surface-integrated photonic crystal, Fig. 1(b),(c) correspond to the close-range top view of the SiPM with TPC constructed on the surface and the schematic diagram of the three-dimensional structure of the topological photonic crystal, respectively, Fig. 1(d) is the schematic view of the cross-section of the SiPMs with TPC constructed on the surface, Fig. 1(e) is the schematic view of TPC two-dimensional lattice arrangement, Fig. 1(f) defines the geometric structure of a single lattice unit for band analysis, and Fig. 1(g) is the sketch of photon propagation path in the topological edge state.

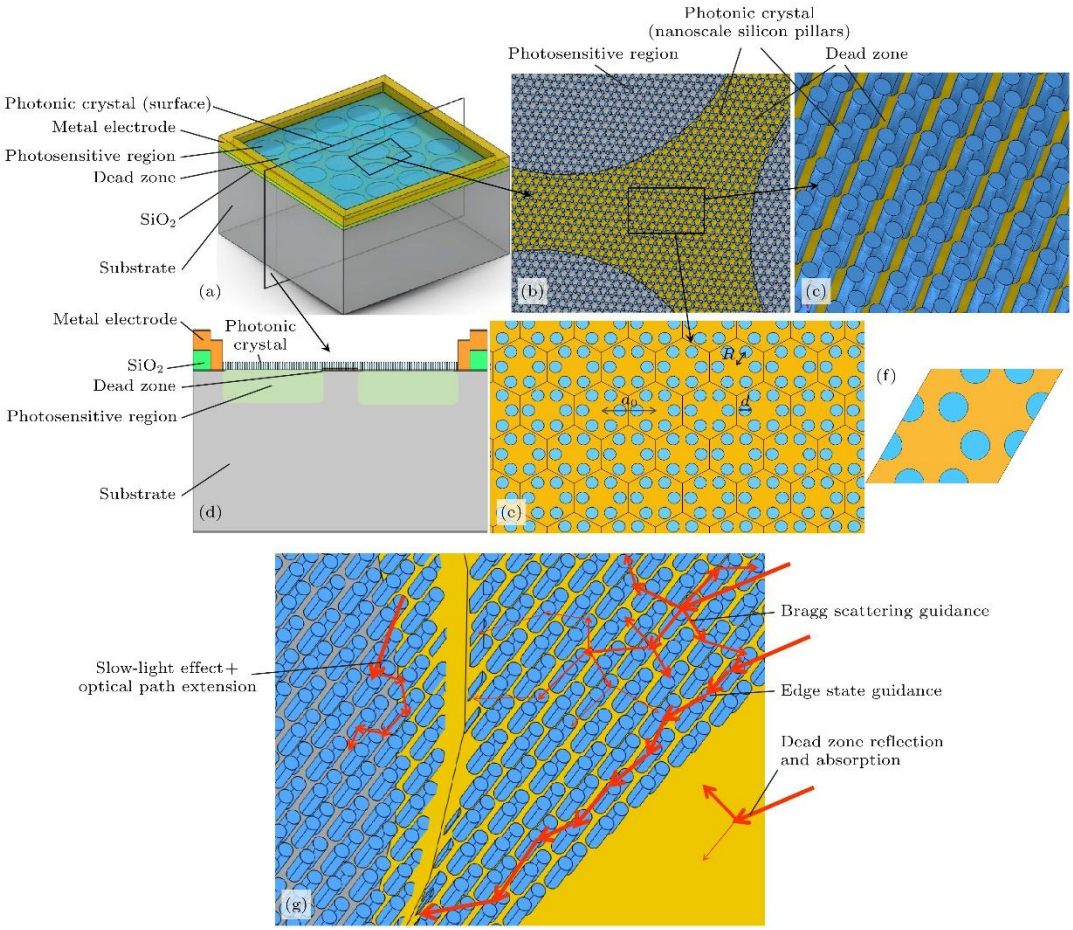

Figure 1. Schematic diagrams of the principle of constructing topological photonic crystals on the surface of SiPM: (a) Schematic diagram of the three-dimensional structure of SiPM; (b) close-up top view; (c) schematic diagram of topological insulating photonic crystal (close-up); (d) two-dimensional cross-sectional schematic diagram of SiPM with topological photonic crystals on the surface; (e) schematic diagram of TPC two-dimensional lattice; (f) schematic diagram of Floquet periodicity analysis; (g) schematic diagram of photon propagation in TPC.

3. Theoretical modeling

Based on the two photon control mechanisms realized by constructing the topological insulating photonic crystal in the dead zone and the photosensitive zone described in Section2, it is necessary to establish corresponding theoretical models in the two zones respectively to quantitatively analyze the improvement mechanism of the photon detection efficiency. The theoretical model of the dead zone is as follows:

$$P_{guide}(\lambda) = \frac{P_{trap}(\lambda)}{P_{in-dead}(\lambda)} \tag{1}$$

$$F_{eff}(\lambda) = f_{active} + f_{dead} \cdot P_{guide} \tag{2}$$

$$K_{guide}(\lambda)=\frac{F_{eff}(\lambda)}{f_{active}}=1+\frac{f_{dead}\cdot P_{guide}(\lambda)}{f_{active}} \tag{3}$$

Where $P_{\text{guide}}(\lambda)$ represents the probability that a photon is directed into the photosensitive region, $P_{\text{trap}}(\lambda)$ is the integral of the optical power flux over the boundaries of the photosensitive surface, and $P_{\text{in-dead}}(\lambda)$ is the total power incident on the dead zone. f_{active} and f_{dead} represent the proportion of photosensitive area and the proportion of dead area, respectively, F_{eff} is the effective GFF, and $K_{\text{guide}}(\lambda)$ represents the enhancement coefficient of the effective GFF.

The topological photonic crystal is introduced in the photosensitive region, and the theoretical model is as follows:

$$G_{\text{path}}(\lambda)=\frac{\eta_{\text{abs}}^{(\text{topo})}}{\eta_{\text{abs}}^{(\text{base})}} \tag{4}$$

$$\begin{cases}\eta_{\text{abs}}^{(\text{base})}=1-e^{-\alpha(\lambda)\cdot L_0}\\ \eta_{\text{abs}}^{(\text{topo})}=1-e^{-\alpha(\lambda)\cdot L_0\cdot k(\lambda)}\end{cases} \tag{5}$$

$$k(\lambda)=\left(\frac{n_{\text{eff}}(\lambda)}{n_{\text{bare}}}\right)\cdot\left(\frac{L_{\text{topo}}(\lambda)}{L_0}\right) \tag{6}$$

Where $G_{\text{path}}(\lambda)$ is the single-photon absorption efficiency enhancement coefficient factor, L_0 is the original active region silicon layer thickness (assuming the optical path is normal incidence), $L_{\text{topo}}(\lambda)$ is the photon path length after introducing the topological photonic crystal in the photosensitive region (obtained from simulation), $\alpha(\lambda)$ is the wavelength-dependent absorption coefficient of silicon (obtained in [14]), and $\eta_{\text{abs}}^{\text{base}}$ is the absorption efficiency of the initial SiPM, and $\eta_{\text{abs}}^{\text{topo}}$ is the absorption efficiency after introducing the TPC in the photosensitive region. Here, $k(\lambda)$ is a dimensionless coefficient (related to the characteristics of the TPC) that converts the lateral path $L_{\text{topo}}(\lambda)$ into an equivalent factor for the longitudinal equivalent absorption path, incorporating both the slow-light effect and the lateral propagation path. $n_{\text{eff}}(\lambda)$ is the effective refractive index (obtained from simulations), and $n_{\text{bare}}(\lambda)$ is the refractive index of bare silicon.

The above two mechanisms are coupled into the PDE model of the SiPM:

$$PDE_{\text{topo}}(\lambda)=PDE_{\text{base}}(\lambda)\cdot G_{\text{total}}(\lambda) \tag{7}$$

$$G_{\text{total}}(\lambda)=K_{\text{guide}}(\lambda)\cdot G_{\text{path}}(\lambda) \tag{8}$$

$PDE_{base}(\lambda)$ is the original PDE curve, $G_{total}(\lambda)$ is the PDE enhancement coefficient of the topological insulating photonic crystal built on the SiPM surface, and $PDE_{toal}(\lambda)$ is the PDE of the TPC built on the SiPM surface.

4. Simulation method

In the COMSOL simulation, the characteristic frequency analysis is first carried out by using the electromagnetic wave frequency domain module to verify the band inversion characteristics of a single lattice unit. The band structure (Fig. 2) of the lattice structure shown in Fig. 1(f) is obtained by Floquet periodicity analysis at different wave vectors. Subsequently, the feasibility simulation of transverse electromagnetic wave mode (Fig. 3) is carried out for the optical field propagation characteristics of multiple lattice units in the three-dimensional structure.

In the two-dimensional simulation, the TPC structure in the dead zone region is first simulated in the full-band (300 — 1100 nm) frequency domain (Fig. 4) with multiple incident light sources, and the enhancement coefficient of the effective GFF $K_{guide}(\lambda)$ is obtained by calculating the ratio of the power flow integral on the photosensitive region boundary to the total incident power. Then, the average propagation path length $L_{topo}(\lambda)$ of photons in the photosensitive region structure (Fig. 5) is extracted, and the gain factor $G_{path}(\lambda)$ of single pixel absorption efficiency is calculated by combining the wavelength-dependent absorption coefficient $\alpha(\lambda)$ of silicon material. Finally, the dead zone is coupled with the enhancement effect of the photosensitive region to obtain the enhancement effect of the overall PDE (Fig. 6).

The simulated SiPM unit structure parameters using honeycomb lattice are as follows: the diameter of a single G-APD unit is 10 μm, the distance between the centers of adjacent units is 13 μm, the narrowest width of the dead zone is 3 μm, the corresponding photosensitive region area ratio f_{active} = 46.4%, the dead zone ratio f_{dead} = 53.6%, the lattice constant a_0 = 300 nm, $R = a_0/2.9$, and the diameter of the Si column $d = 2R/3$. The selection of these key TPC parameters is based on literature support and principles of device adaptation optimization: Reference [13] (a seminal work in the field of topological photonic crystals) indicates that the silicon pillar diameter (d=2R/3) ensures optimal dielectric contrast of the lattice, and $a_0/R = 2.9$ enables the formation of a topological bandgap covering the 460—1100 nm range, which aligns with the target modulation wavelength band of this paper. Tailored to the characteristics of SiPM devices, the lattice constant ($a_0 = 300$ nm) was determined through parameter sweeping in COMSOL. This value is compatible with the minimum dead region width of 3 μm (accommodating 10 lattice periods to prevent truncation of the topological edge state by the boundary), while also avoiding the influence of the structural photonic bandgap at wavelengths below 460 nm. Furthermore, this parameter is compatible with the standard process of epitaxially growing a high-resistivity epilayer on a low-resistivity substrate.

5. Simulation Results and Analysis

The results of the eigenfrequency analysis of the smallest lattice unit (Fig. 1(f)) of the TPC are as follows. The Fig. 2(a) —(c) shows the band distribution of the single lattice structure of TPC, and the phenomenon of band gap and band inversion can be observed near the wavelength of 621 nm, which is consistent with the report of reference [13], thus verifying the topological non-triviality of the lattice structure. When the λ = 621 nm, the Fig. 2(d) shows the electric field distribution at the boundary, which verifies the control effect of TPC on the boundary state propagation of photons. When λ = 900 nm, the Fig. 2(e) shows that the electric field is mainly localized in the central region of the silicon pillar, and the edge localization is weak, which reflects the Bragg guiding mechanism of the TPC for photons. When λ = 460 nm, the pure bulk electric field shown by Fig. 2(f) is completely localized inside the silicon pillar, and no obvious field distribution is observed at the boundary. The electric field distribution patterns at the above three typical wavelengths clearly reveal the photon control ability of the topological photonic crystal in different frequency bands, and further prove the mechanism of the synergistic mechanism of "topological boundary state guiding + Bragg scattering enhancement" in the broad spectral response.

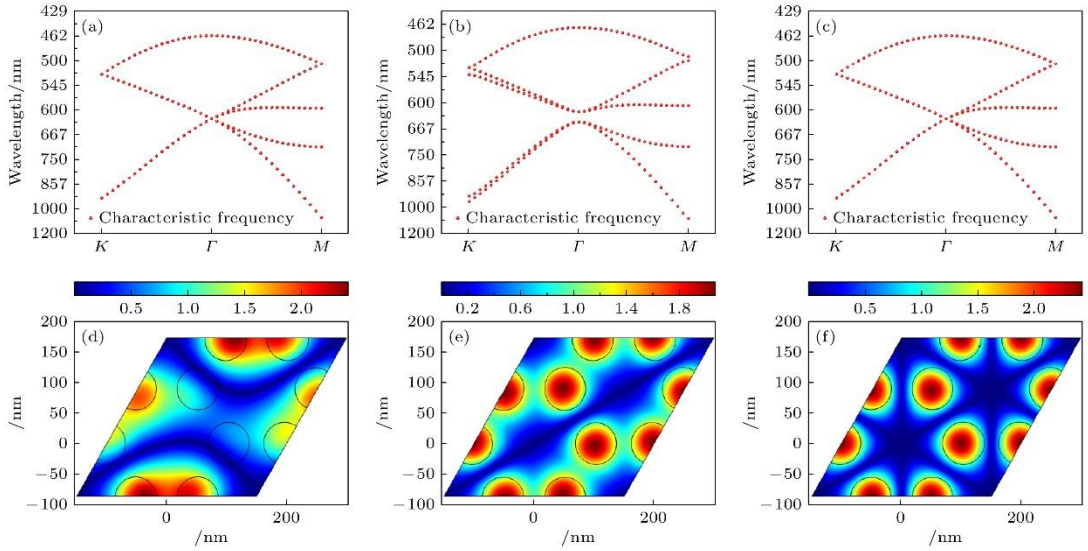

Figure 2. Energy band diagrams of a single lattice structure of topological insulating photonic crystals: (a) $R = a_0/3$; (b) $R = a_0/2.9$; (c) $R = a_0/3.1$; (d) boundary state; (e) Bragg scattering bulk state; (f) electric field mode distribution of pure bulk state (unit: V).

The Fig. 3 is the three-dimensional simulation structure diagram of the topological photonic crystal. Under the condition of normal incidence (Fig. 3(a)), the electric field intensity of the electromagnetic wave is significantly localized near the Si pillar at a distance of about 10 nm from the SiPM surface, while the electric field intensity in the air region is relatively low. This phenomenon indicates that the periodic arrangement of Si pillars effectively couples the

electromagnetic wave energy into the transversely propagating guided mode. Since the transverse size of Si pillars (about 60 nm in diameter) is smaller than the wavelength of the incident light (300 — 1100 nm), the longitudinal field variation of Si pillars can be reasonably ignored in the long wavelength band (λ > 600 nm), which satisfies the long-wave approximation; In the short wavelength range (λ < 600 nm), the transverse guided modes are effectively confined by the band structure design of the photonic crystal. Based on the above characteristics, the two-dimensional simulation model combined with the plane wave expansion method or finite element method to solve Maxwell's equations can accurately capture the band inversion behavior of the lattice and the transmission characteristics of the topological edge States, thus providing reliable theoretical support for the photonic control mechanism of the device.

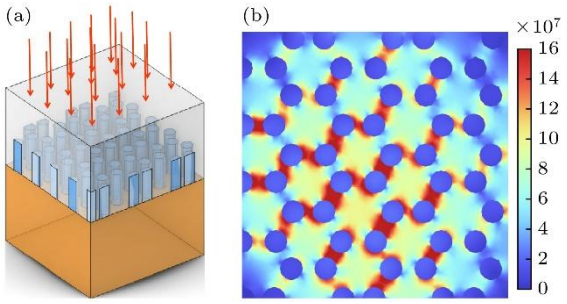

Figure 3. Three-dimensional simulation structure diagrams: (a) Geometric modeling; (b) electric field mode distribution of photonic crystals (unit: V).

The optical propagation path (electric field distribution) of the TPC is constructed in the dead zone at different wavelengths (460 nm, 550 nm, 621 nm, 650 nm, 700 nm, 800 nm, 900 nm, 1100 nm) with Fig. 4. From the electric field distribution, it can be seen that the propagation path of photons in the dead zone shows a specific mode related to the wavelength. As shown in the Fig. 4(i), at the wavelength of 621 nm, the electric field distribution clearly reveals the existence of topological boundary States, and the directional transmission of photons along the lattice interface is achieved, which is due to the topologically protected edge States induced by the band inversion characteristics of TPC, showing excellent scattering-free transmission ability. The 460 — 700 nm band (Fig. 4(a) —(e)) is located in the topologically protected frequency band corresponding to the band inversion, and although the edge state is not strictly single-mode propagation, it still shows strong anti-scattering ability; At the same time, the periodic dielectric distribution of the honeycomb lattice in the dead zone of this band stimulates Bragg scattering, which reduces the reflection loss of photons to the metal surface, and the two cooperate to effectively guide photons to the photosensitive region, thus improving the effective GFF. However, for the wavelength range of 700 — 1100 nm (Fig. 4(f) —(h)), the periodic dielectric distribution of the honeycomb TPC structure suppresses the light reflection from the metal surface mainly through the Bragg scattering mechanism, so that some photons enter the photosensitive region through non-edge state paths (such as diffraction or multiple scattering). This mechanism expands the photon

capture ability of the dead zone and enhances the response performance of the device in the long wavelength band.

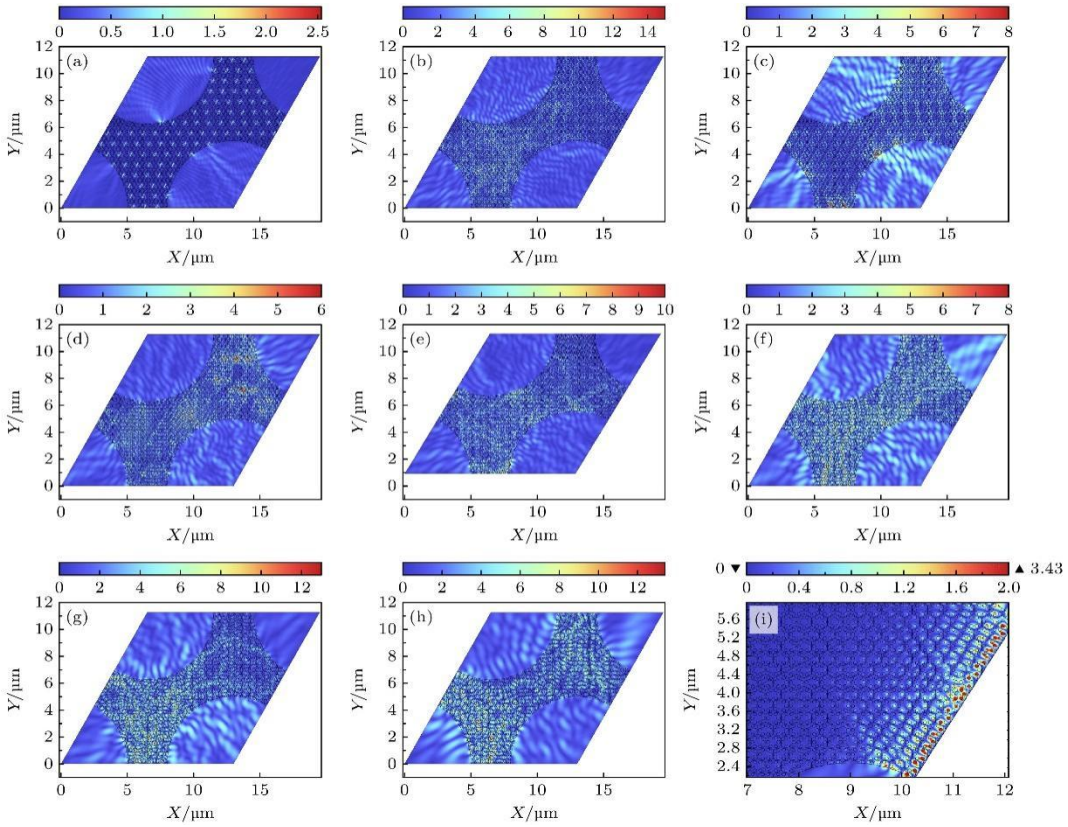

Figure 4. Electric field mode distribution diagrams of TPC constructed in the dead zone (unit: V) at different wavelengths: (a) 450 nm; (b) 550 nm; (c) 621 nm; (d) 650 nm; (e) 700 nm; (f) 800 nm; (g) 900 nm; (h) 1100 nm; (i) boundary state propagation at 621 nm wavelength.

The results of electromagnetic field distribution at different wavelengths show that the topological photonic crystal realizes the ability of wavelength selectivity control in the dead zone and realizes efficient photon transmission in a wide spectral range through the synergistic mechanism of "topological edge state guidance + Bragg scattering enhancement". This structure not only improves the coupling efficiency of photons from the dead zone to the photosensitive zone, but also lays a physical foundation for the optimization of the overall detection performance of SiPM. In addition, due to the defect-resistant transmission characteristics of the topological photonic crystal, the scattering loss caused by structural defects can be effectively avoided during the photon propagation in the dead zone, and a stable transmission path can be maintained. Even if there are lattice defects in the actual preparation, the robustness of the topological structure can still ensure that the photon propagation mode is not significantly affected by[11–13], thus ensuring the efficiency and stability of the dead-zone photon transmission.

The Fig. 5 is the optical propagation path (electromagnetic wave electric field distribution) of the TPC constructed in the photosensitive region at different wavelengths (460 nm, 550 nm, 650

nm, 700 nm, 900 nm, 1100 nm). These electric field distribution images clearly show the propagation path of photons in the photosensitive region. On the one hand, the TPC periodic silicon pillars extend the transverse propagation path of photons through the slow light effect, and extend the interaction time between photons and silicon materials; On the other hand, the periodic dielectric distribution of silicon pillars stimulates Bragg scattering[11], reduces the surface reflection loss of the photosensitive region, and further enhances the absorption efficiency of photons in the photosensitive region. This synergistic mechanism not only improves the photon capture ability in a wide spectral range, but also provides a key support for the optimization of the overall detection performance of SiPM, which is one of the important physical mechanisms to achieve the enhancement of its wide spectral response.

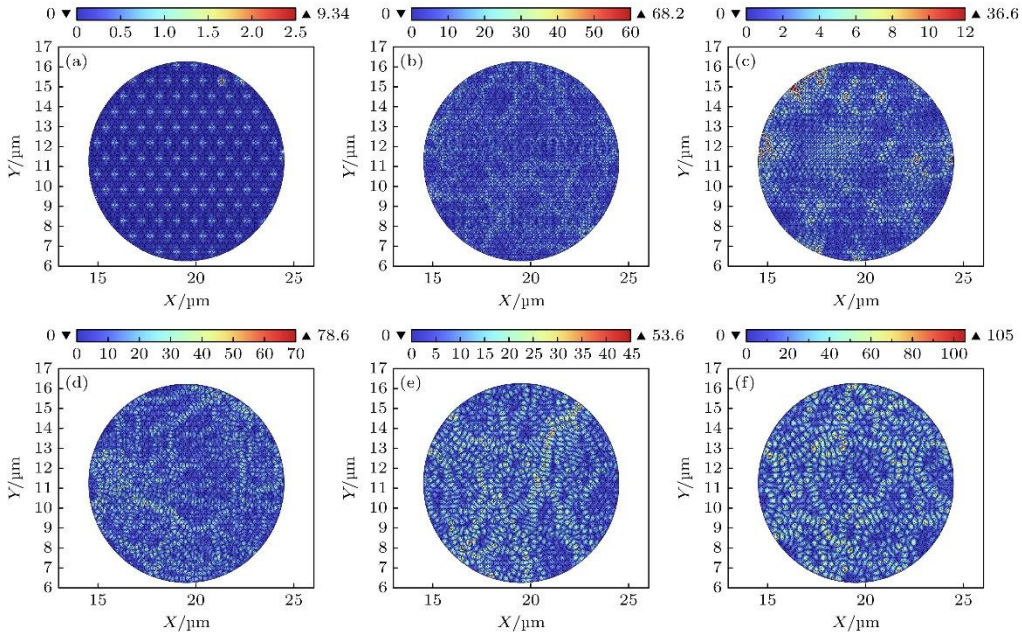

Figure 5. Electric field mode distribution diagrams of TPC constructed in the photosensitive region (unit: V) at different wavelengths: (a) 460 nm; (b) 550 nm; (c) 650 nm; (d) 700 nm; (e) 900 nm; (f) 1100 nm.

Fig. 6 is the curve of enhancement coefficient as a function of wavelength. The black curve is the GFF enhancement coefficient K_{guide} (λ), the red curve is the absorption efficiency enhancement coefficient G_{path} (λ), and the blue curve is the PDE enhancement coefficient G_{total} (λ). It can be seen that the effective GFF is increased from 46.4% of the original structure to 46.4% — 63.1% at different wavelengths, and the absorption efficiency of a single pixel is increased by 0% — 60%. At λ< 600 nm, due to the high carrier recombination rate in the highly doped region of the photosensitive silicon material, the further improvement of the photon absorption efficiency is limited. At λ> 600 nm, the photon absorption efficiency in the photosensitive region increases with

the increase of wavelength. TPC significantly enhances the absorption efficiency of photons in the photosensitive region through the slow light effect and the extension of the optical path. This application has been studied in solar cells[15–17]. Although the slow light effect and optical path extension of TPC have limited enhancement of absorption efficiency in the $\lambda < 600$ nm band, the increase of effective GFF still contributes to the improvement of overall PDE. However, in the wavelength region less than 460 nm, the TPC structure has a photonic band gap effect, which hinders the propagation of photons in it, so the promotion effect on PDE is negligible. In contrast, the dead zone (increasing the effective GFF) and the photosensitive surface (increasing the absorption efficiency, related to IQE) of the TPC can increase the PDE of the SiPM by about 50% on average in the range of 460-1100 nm.

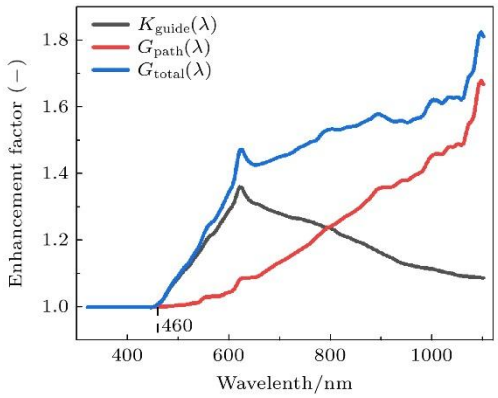

Figure 6. Curve of enhancement factor varying with wavelength.

The black curve in Fig. 7 corresponds to the experimental test PDE data of SiPM without TPC structure, and the red solid line is the PDE simulation curve of SiPM with TPC structure on the surface, which is the calculation result based on the (8) formula. The black curve is the experimental test PDE data of the SiPM without TPC structure (see reference [18] for the test method). The detector used in the test is a self-developed SiPM, and its G-APD unit parameters (such as unit diameter of 10 μm and center spacing of 13 μm) are consistent with the simulation parameters in this paper, and the number of units is 4. It can be seen that the PDE of SiPM is improved in the wavelength range of 460-1100 nm. The above results intuitively demonstrate the enhancement of SiPM detection efficiency by TPC in a wide spectral range and its significant wavelength dependence.

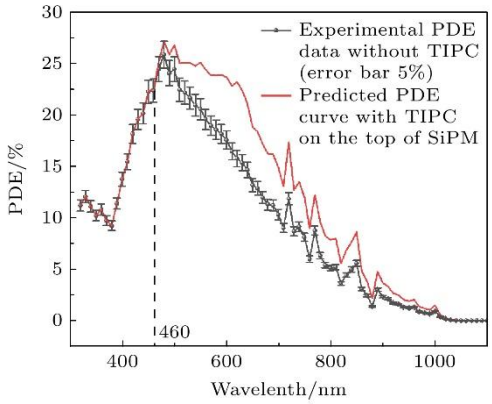

Figure 7. Comparison of PDE curves of SiPM with and without surface topological photonic crystal structure.

6. Discussion

Fig. 8 shows the SiPM fabrication process flow chart of SiPM surface integrated TPC, which is compatible with the existing SiPM passivation layer process, and the technology selection of each step can be adapted as required. The specific analysis is as follows. The method comprise that steps of: firstly, carry out plasma enhanced chemical vapor deposition (PECVD) on an ion implanted silicon wafer to deposit a 200-300 nm amorphous Si film (the temperature is less than or equal to 200 deg C, and the SiH_4 flow rate is 50 mL/min unde a standard condition), wherein the step is directly connected with an existing pretreatment process; Subsequently, the dead zone and photosensitive zone honeycomb lattice structure (a_0 = 300 nm, $R = a_0/2.9$, silicon pillar diameter $2R/3$ nm) was defined by electron beam lithography[19] (accelerating voltage 20 keV, dose 120 μC/cm^2) or deep ultraviolet lithography[20] (248 nm/193 nm). The precision of electron beam lithography is ± 5 nm, which can meet the requirement of topological symmetry, but its exposure speed is low (about 1 cm^2/h); If mass production is needed, deep ultraviolet lithography can increase the exposure speed by 50-100 times, reduce the cost to 1/20 of the electron beam, and still meet the accuracy requirement of ± 5 nm; If the accuracy and cost are balanced, the "nanoimprint lithography + UV curing"[21] process (speed >10 cm^2/min, accuracy ± 3 nm, equipment investment 1/5 of the electron beam) is more suitable for large-scale manufacturing.

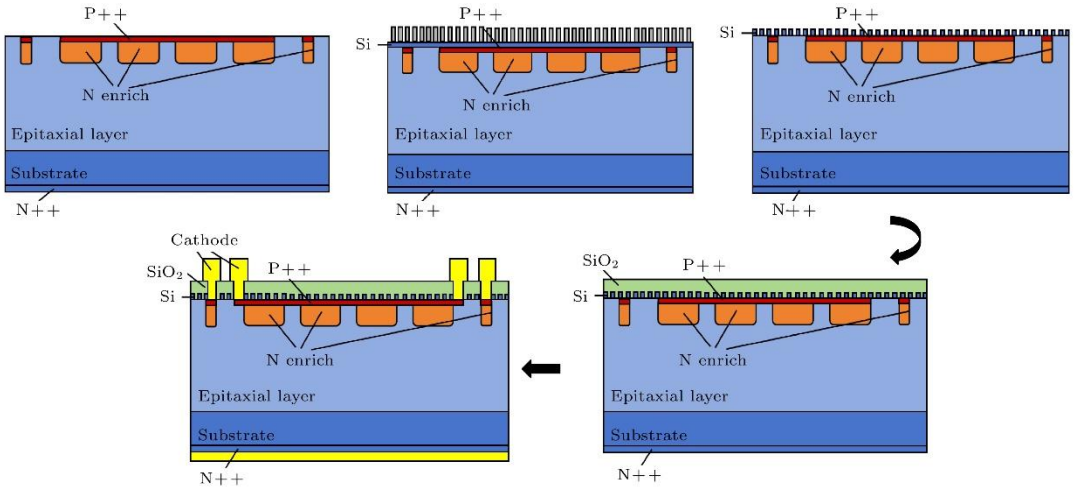

Figure 8. Flow chart of the manufacturing process of SiPM with surface-integrated TPC.

After the photolithography step, the etching depth was controlled by monitoring the intensity of the Si characteristic peak (780 nm) by optical emission spectroscopy using CHF_3/O_2 (3 ∶ 1) reactive ion etching (power 150 W, pressure 10 mTorr) to ensure that the etching reached the bottom of the Si film; The process only needs to add one photolithography-etching, and does not need to reconstruct the existing process system. Compared with the plasmon-dependent extreme ultraviolet lithography process, the equipment cost is reduced by 70%, and metal oxidation can be effectively avoided. Finally, metal electrode evaporation and SiO_2 passivation are completed, which is fully compatible with the SiPM standard post-process. To sum up, the process flow shown in the Fig. 8 achieves a good balance between accuracy, efficiency and cost, which not only meets the structural requirements of the TPC lattice, but also provides a feasible path for the integration of TPC and SiPM by simplifying the complex process of the traditional scheme. Furthermore, reference [15] verifies the significant improvement of the sensitivity of the electro-optic polymer-based optical phase modulator in a wide wavelength range through the structural design of 1D and 2D photonic crystals, which provides practical support for the application of photonic crystals in the performance optimization of optoelectronic devices; In reference [16], the process compatibility of photonic crystal solar cells is reviewed, and it is clearly pointed out that ultraviolet lithography is the key technology to realize large-scale periodic structures; Reference [17] proves the excellent performance of double-sided iridescent high-efficiency perovskite solar cells and modules with inverse opal photonic crystal structure in the near-infrared band through the combination of simulation and experiment, which further proves the enhancement effect of photonic crystal structure on wide spectral response. This series of studies not only verify the feasibility of TPC structure at the experimental level, but also provide a key reference for subsequent process optimization and industrial application.

Comparison of the effects of different methods for improving the PDE of SiPM by Tab. 1. It can be seen that the method proposed in this paper has certain advantages. The method of constructing topological photonic crystal on the surface of SiPM achieves an average increase of

50% in PDE in the 460-1100 nm band through the synergistic effect of "dead zone photon guidance + photosensitive zone absorption efficiency improvement", in which the effective GFF is significantly increased from 46.4% to 63.1% at 621 nm due to the unidirectional propagation characteristics of TPC edge States and the synergistic effect of Bragg scattering excited by periodic dielectric distribution of dead zone honeycomb lattice to reduce reflection loss on the metal surface; At 900 nm, the absorption efficiency is increased from 41. 19% to 55. 94% due to the reduction of reflection loss, optical path extension effect and slow light effect of honeycomb lattice Bragg resonance. In contrast, the microlens array improves the PDE value by 24% only through the geometric reorientation method, which is significantly dependent on the wavelength, and the improvement is only less than 10% above 900 nm. The wavelength range of plasmon response is about 1/3 of that of topological insulating photonic crystal.

Table 1. Comparison of methods for improving the PDE of SiPM.

Document	Optimization method	Band response range/nm	PDE lift	Process complexity	Lifting peak
[7]	Spherical microlens array	400—900	24%	High	24% (400—900 nm)
[22]	Cylindrical microlens array	450—650	About 50%	High	50% (450—650 nm)
[23]	Diffractive microlens array	500—900	—	High	—
[24]	Plasmon	600—850	150% in 660-690 nm and less than 30% in other bands	Extremely high	170% (675 nm)
The present work	Topological photonic crystal	460—1100	50% (average)	Medium	81% (1100 nm)

In order to verify the influence of the etching error of the silicon pillar diameter in the process, based on the COMSOL electromagnetic wave frequency domain module, the deviations of ± 5 nm and ± 10 nm are introduced to the silicon pillar diameter respectively (the original design diameter ($d \approx 61.4$ nm) is known, the corresponding $d = 2R/3$, and the $a_0 = 300$ nm), and the influence on the PDE in the 460 — 1100 nm band is simulated and analyzed. The results are shown in Tab. 2.

Table 2. Influences of silicon pillar diameter etching errors on SiPM PDE.

Silicon pillar diameter deviation	effective GFF/% at 621 nm	absorption efficiency at 900 nm/%	Average increase/% of PDE in 460-1100 nm band
Error-free (original design)	63.10	51.37	50
±5 nm	61.46	49.85	48.5
±10 nm	59.29	48.27	46.8

It can be seen from the Tab. 2 that the influence of the etching error of the silicon pillar diameter on the PDE changes in a gradient manner: when the deviation is ± 5 nm (mainstream process accuracy), the effective GFF of 621 nm decreases from 63.10% to 61.46% (down by

1.64%), the absorption efficiency of 900 nm decreases from 51.37% to 49.85% (down by 1.52%), and the PDE in the 460-1100 nm band still increases by 48.50% on average (only down by 1.50%). because the change in the dielectric contrast of the lattice is less than 3%, and core mechanisms such as TPC edge states and slow-light effects remain stable. When the deviation expands to ±10 nm (beyond-normal fluctuation), the effective GFF decreases by 3.81%, the absorption efficiency decreases by 3.10%, and the average PDE improvement drops to 46.80%. However, this is still significantly better than the improvement offered by traditional microlenses (24%), reflecting the robustness of TPC to process errors. Even if part of the lattice periodicity deviates, the topological defect immunity (validated in reference [13]) can still maintain core functionality, avoiding sharp performance degradation.

7. Conclusion

It is proved by theory and simulation that the photon detection efficiency of SiPM can be improved by fabricating topological photonic crystal structure on the surface of silicon photomultiplier chip. The PDE of SiPM in the wide spectral band of 460 — 1100 nm can be effectively improved by introducing the TPC structure designed in different regions, and the PDE in this band can be improved by 50% on average, and the peak value can reach 81%. The band inversion of TPC can induce the formation of topological edge States, reduce the reflection loss of metal surface by exciting Bragg scattering in the dead zone based on the periodic dielectric distribution of honeycomb lattice, superimpose the anti-defect transmission and directional scattering effect of edge States, and significantly improve the effective coupling efficiency of photons to the photosensitive region; In the photosensitive region, the periodic silicon pillar structure extends the transverse propagation path of photons through the slow light effect, and reduces the surface reflection by means of the periodic Bragg scattering effect of the lattice, which forms a synergistic effect with the absorption characteristics of the silicon material, thus further enhancing the long-band photoresponse performance. In addition, the robustness of the topology effectively reduces the dependence on the preparation accuracy, which can be achieved by using the mainstream etching process (electron beam lithography + reactive ion etching), and has excellent process compatibility. This study provides a new idea based on topological photonics for the spectral response optimization of solid-state photodetectors, which can be combined with experimental verification and device integration technology to promote their practical application in the field of high-performance photodetection in the future.

References

[1] Zhao B, Huang Y, Wang C 2024 Nucl. Instrum. Methods Phys. Res. Sect. A 1059 168975

[2] Rignanese L P, Antonioli P, Preghenella R, Scapparone E 2024 La Riv. Nuovo Cimento 47 299

[3] Herbert D J, Saveliev V, Belcari N, Bisogni M G, Del Guerra A, Golovin A 2004 IEEE Nuclear Science Symposium Conference Record Rome, Italy, October 16–22, 2004 p4185

[4] Yan T Y, Wang X Y, Liu S T, Fan D W, Xu X Y, Zeng Q, Xie H, Yang X L, Zhu S P, Ma X P, Yuan Z, Chen X L 2022 Small Methods 6 2201105

[5] Okino T, Yamada S, Sakata Y, Kasuga S, Takemoto M, Nose Y, Koshida H, Tamaru M, Sugiura Y, Saito S, Koyama S, Mori M, Hirose Y, Sawada M, Odagawa A, Tanaka T 2020 IEEE International Solid-State Circuits Conference (ISSCC) San Francisco, CA, USA, February 16–20, 2020 p9063045

[6] Baker-Finch S C, McIntosh K R, Yan D, Fong K C, Kho T C 2014 J. Appl. Phys. 116 063101

[7] Haefeli G, Blanc F, Currás-Rivera E, Marchevski R, Ronchetti F, Schneider O, Shchutska L, Trippl C, Zaffaroni E, Zunica G 2024 arXiv: 2411.09358 [hep-ex]

[8] Álvarez-Garrote R, Calvo E, Canto A, Crespo-Anadón J I, Cuesta C, de la Torre Rojo A, Gil-Botella I, Manthey Corchado S, Martín I, Palomares C, Pérez-Molina L, Verdugo de Osa A 2024 Nucl. Instrum. Methods Phys. Res. Sect. A 1064 169347

[9] Villa F, Bronzi D, Vergani M, Zou Y, Ruggeri A, Zappa F, Dalla Mora A 2014 European Solid-State Device Research Conference (ESSDERC) Grenoble, France, September 22–26, 2014 p294

[10] Wang Y, Chen Z D, Li C H, He R, Wang S Y, Li B C, Wang R H, Liang K, Yang R, Han D J 2015 Nucl. Instrum. Methods Phys. Res., Sect. A 787 38

[11] Jia D, Ge Y, Yuan S Q, Sun H X 2019 Acta Phys. Sin. 68 224301

[12] Lu H, Tian H P, Li C H, Ji Y F 2009 Acta Phys. Sin. 58 2049

[13] Wu L H, Hu X 2015 Phys. Rev. Lett. 114 223901

[14] Cui H Y, Li Z F, Ma F J, Chen X S, Lu W 2010 Acta Phys. Sin. 59 7055

[15] Xiao L, Lei T Y, Liang Y, Zhao M, Liu H, Zhang S Q, Li H, Ma J, Wu X Y 2016 Acta Phys. Sin. 65 134207

[16] Zhao C, Ma Y, Wang Y, Zhou X, Li H Z, Li M Z, Song Y L 2018 Acta Chim. Sin. 76 9

[17] Zou S W, Xin Y, Jin J L, Lin Z C, He Y Y, Liang J, Yan X J, Huang J M 2025 Adv. Mater. 37 2410130

[18] Wang Y, Yang Y F, Wu Y, Wang L, Liu L, Liu L N, Li L B, Han X X, Li Z B, Zhang G Q 2024 Proceedings of SPIE San Diego, CA, USA, August 12–16, 2024 p13283

[19] Zheng Y, Gao P P, Tang X, Li J, Liu Y, Zhang H 2022 J. Cent. South Univ. 29 3335

[20] Mao S S, Li Y Q, Jiang J H, Shen S H, Liu K, Zheng M 2018 Chin. Opt. Lett. 16 030801

[21] Zhou W M, Min G Q, Zhang J, Liu Y B, Wang J H, Zhang Y P, Sun F 2011 Nano-Micro Lett. 3 135

[22] Gyongy I, Davies A, Gallinet B, Dutton N A W, Duncan R R, Rickman C, Henderson R K, Dalgarno P A 2018 Opt. Express 26 2280

[23] Intermite G, McCarthy A, Warburton R E, Ren X, Villa F, Lussana R, Waddie A J, Taghizadeh M R, Tosi A, Zappa F, Buller G S 2015 Opt. Express 23 33777

[24] Duan Q L, Liu Y, Chang S S, Chen H Y, Chen J H 2021 Sensors 21 5262